Selective inhibitors of SIRT2 regulate perinuclear α-tubulin acetylation, migration, and invasion of breast cancer cells

Alexander L. Nielsen,[1] Nima Rajabi,[1] Norio Kudo,[2] Kathrine Lundø,[3] Martin Fontenas,[1] Alessia Lucidi,[1] Andreas S. Madsen,[1,†] Minoru Yoshida,[2] and Christian A. Olsen[1,*]

ABSTRACT

Sirtuin 2 (SIRT2) is a protein deacylase enzyme that has been reported to remove both acetyl groups and longer chain acyl groups from lysine residues in post-translationally modified proteins. It affects diverse biological functions in the cell and has been considered a drug target in relation to both neurodegenerative diseases and cancer. Therefore, access to good chemical tool compounds are essential for the continued investigation of the complex function of this enzyme. Here, we report a collection of probes that are potent, selective, stable in serum, water soluble, amenable to cell culture experiments, and inhibit both SIRT2 deacetylation and demyristoylation. Compared to the current landscape of SIRT2 inhibitors, this is a unique ensemble of features built into a single compound. We expect the developed chemotypes to find broad applications in the interrogation of SIRT2 functions in both healthy and diseased cells to provide a foundation for the development of new therapeutics in the future.

Keywords: Sirtuins, SIRT2, posttranslational modifications, enzyme inhibitors, X-ray crystallography

[1]Center for Biopharmaceuticals & Department of Drug Design and Pharmacology, Faculty of Health and Medical Sciences, University of Copenhagen, Universitetsparken 2, DK-2100, Copenhagen, Denmark. [2]RIKEN Center for Sustainable Resource Science (S13), Hirosawa 2-1, Wako, Saitama 351-0198, Japan. [3]Novo Nordisk Foundation Center for Basic Metabolic Research, Faculty of Health and Medical Sciences, University of Copenhagen, Blegdamsvej 3B, DK-2200, Copenhagen, Denmark. †Present address: Novo Nordisk A/S, DK-2880, Bagsværd, Denmark. *email: cao@sund.ku.dk.

Introduction

The sirtuins are NAD^+-dependent lysine deacylase enzymes that are highly conserved across species with seven isoforms (SIRT1–7) present in humans. These enzymes all have an NAD^+-binding pocket and catalytic core, but have different cellular expression profiles, subcellular localization, and substrate specificities.[1,2] Sirtuins were originally reported as being ε-*N*-acetyllysine (Kac) hydrolases, but in recent years, it has become evident that a variety of ε-*N*-acyllysine posttranslational modifications (PTMs) can be removed by sirtuins[3–8] as well as zinc-dependent histone deacetylases (HDACs).[9–14] These findings formed the basis of a paradigm shift in the understanding of lysine modifications and their influence on cell signaling and implication in disease.[15] Sirtuin 2 is predominantly localized to the cytosol where it is believed to act mainly as a deacetylase of microtubular proteins such as α-tubulin,[16,17] serving as a regulator in cell division and proliferation.[18,19] However, SIRT2 has been shown to have a much broader substrate scope, with a preference for long chain acyl groups (C_6–C_{16}) *in vitro*[5,20,21] and recently also shown to target lysine benzoylation (Kbz).[22] Generally, SIRT2 has been recognized as a tumor suppressor[23] but knockdown and inhibition of SIRT2 have also been shown to have broad anticancer activity in human breast cancer cell lines by promoting c-Myc degradation.[24] Additionally, SIRT2 has been linked to neurodegeneration[25,26] and has been shown to promote lipolysis and prevent differentiation in mature adipocytes;[27] thus, constituting a potential target of metabolic diseases and obesity.[28,29] Interestingly, both activation and inhibition of SIRT2 appear to have therapeutic potential, depending on the pathway under scrutiny. Accordingly, the complex role of SIRT2 calls for further investigation and development of tool compounds to enable these endeavors.

Numerous SIRT2 inhibitors have been reported recently (Fig. 1),[24,30–48] some of which are commercially available (*i.e.* **SirReal2**, **AGK-2**, **tenovin-6**). However, all of these compounds are endowed with limitations due to lack of isozyme selectivity, potency against demyristoylase activity, or poor solubility. We therefore embarked on a mechanism-based and substrate-mimicking approach to develop novel inhibitors of SIRT2 with improved attributes and efficacy.

Efforts of numerous groups over the last two decades have led to almost 30 X-ray crystal structures, including several co-crystal structures with ligands and inhibitors.[34,35,52–56,36–40,49–51] This has provided insight into the binding mechanism and substrate scope of SIRT2 at the molecular level. In the present work, we have built on this previous knowledge to develop the most potent and selective SIRT2 inhibitors reported to date. These inhibitors were shown to increase perinuclear acetylation levels of α-tubulin in MCF-7 cells and exhibited inhibition of cell migration and invasion of MCF-7 breast cancer cells in culture. Additionally, the data provides valuable insight into the stability of mechanism-based, thioamide- and thiourea-containing sirtuin inhibitors in human serum, which will serve as useful guidance for future studies.

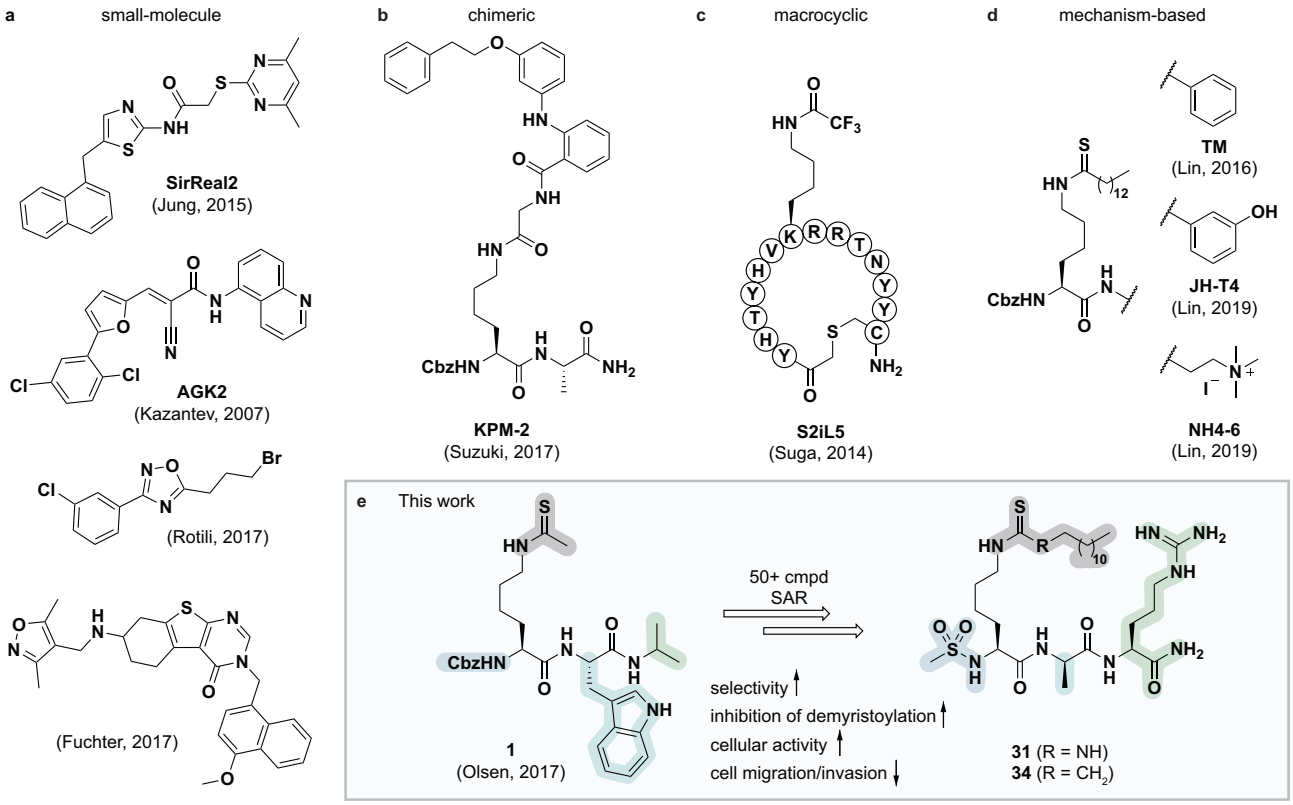

Fig. 1. Representative SIRT2 inhibitors. (**a**) Heterocyclic small molecule inhibitors.[30,35,46,47] (**b**) Chimeric lysine mimic **KPM-2**.[37] (**c**) Peptide macrocycle **S2iL5**.[34] (**d**) Mechanism-based inhibitors.[24,32,40] (**e**) Summary of this study.

Results

Structure–activity relationship study and X-ray crystallography. During our previous structure–activity relationship (SAR) study that targeted SIRT5,[57] we found that thioacetamide **1** (Scheme 1a) did not inhibit SIRT5 but rather exhibited inhibition of SIRT2 (14% at 10 μM) and could therefore serve as a starting point for the development of potent substrate-mimicking inhibitors of SIRT2. While thioacetamide-based compounds had already been reported to inhibit SIRT2,[58,59] we turned our attention to longer-chain acyl groups, inspired by the ε-*N*-thiomyristoyllysine-based inhibitor, **TM**, developed by Lin and co-workers.[24] Similar to our findings for SIRT5, the initial series of compounds (**2**–**5**, Scheme 1b) revealed that thioamide- and thiourea-based ε-*N*-acyllysine mimics (compounds **2** and **3**, respectively) led to highly potent inhibitors. Interestingly, introduction of analogous hydrazide or inverted amide moieties (compounds **4** and **5**, respectively), which have previously been reported to serve as sirtuin inhibitors,[60,61] exhibited only limited inhibition in our assays at 100 μM concentration of the compounds. Because thiourea **3** showed slightly higher potency than thioamide **2**, and because the thiourea modifications can be introduced in a late-stage of the compound preparation, we chose the thiourea moiety for the subsequent compound series.

We then gained inspiration from the X-ray co-crystal structure of SIRT2 bound to the 14-mer macrocyclic inhibitor **S2iL5**,[34] which is an analog of macrocyclic inhibitors discovered by Suga and co-workers using mRNA-display technology.[42] This indicated electrostatic interactions between the

guanidinium group of the arginine in the *i*+2 position (counting from the modified lysine in the inhibitor) and two nearby glutamic acid residues of SIRT2 (E116 and E120), prompting us to extend the scaffold by one additional *C*-terminal amino acid residue. This also enabled a solid-phase peptide synthesis (SPPS) approach, using the Rink amide linker[62] to provide ready access to compounds **6**–**12** (Scheme 1c, for synthesis see Scheme S4). Gratifyingly, potency was improved up to 5-fold by the *i*+2 extension. However, since we anticipated that the negative charge in compound **11** would be detrimental for cellular uptake in subsequent assays, we selected compound **9**, containing an arginine residue in the *i*+2 position for further modification. Reintroduction of a short-chain thioacetyl group (compounds **S1**–**S4**, Scheme S1) led to significantly decreased potency against SIRT2, while displaying respectable inhibition against SIRT1, emphasizing the importance of a longer-chain acyl group to target SIRT2 over SIRT1 and SIRT3.

We then investigated the importance of the *i*+1 residue. In some X-ray co-crystal structures of SIRT2, residues surrounding this position are unresolved due to high flexibility and unstructured binding interactions.[6,35] In particular, amino acids 289–304, which are located at the putative *i*+1 binding region, comprise a SIRT2-specific insertion claimed to be stabilized by—and indeed resolved in the co-crystal structure with—the macrocycle **S2iL5**.[34] We therefore investigated the importance of the *i*+1 residue by varying its charge, steric bulk, and stereochemistry in analogs **13**–**23** (Scheme 1d). In agreement with the expected flexibility of the binding region, we found that all modifications except proline led to potent compounds. It was also found that compounds **21** and **23** exhibited the highest degree of selectivity over SIRT1 and SIRT3 (Scheme 1e). Interestingly, these compounds contained a D-Ala or 2-aminobutyric acid (Aib) moiety, which we anticipated would provide improved stability towards proteolytic enzymes.[63] At this stage, we obtained diffraction quality crystals of SIRT2 with compounds **13** and **23** bound and were able to solve X-ray co-crystal structures of both complexes at 1.7 Å resolution (Fig. 2). Superimposing the two structures revealed highly similar conformations (Fig. 2a,b) as well as high similarity to a previously solved co-crystal structure of SIRT2 with a thiomyristoylated peptide substrate analog bound (Fig. 2c). More pronounced differences were observed when comparing our structures to a structure of the apo form of SIRT2 and the structure with **S2iL5** bound (Fig. 2d). Not surprisingly, the upper zinc-binding domain and substrate binding pocket adopted a tighter conformation when bound to the macrocyclic peptide than our inhibitors, which require accommodation of the long fatty acyl side chain modification in the substrate binding pocket (Fig. 2d), whereas the apo form adopted a more open structure. Generally, the most prominent interactions of our inhibitors were backbone–backbone hydrogen bonds (Fig. 2e), in agreement with those observed from an X-ray co-crystal structure with a thiomyristoylated peptide bound to SIRT2 (Fig. 2f).[6] On the other hand, a recent structure of SIRT2 with a glucose-containing analog of **TM** showed a different binding mode (Fig. 2f),[40] which could help explain the lower potency of **TM** analogs compared to inhibitors with more peptide content, due to loss of backbone–backbone interactions.

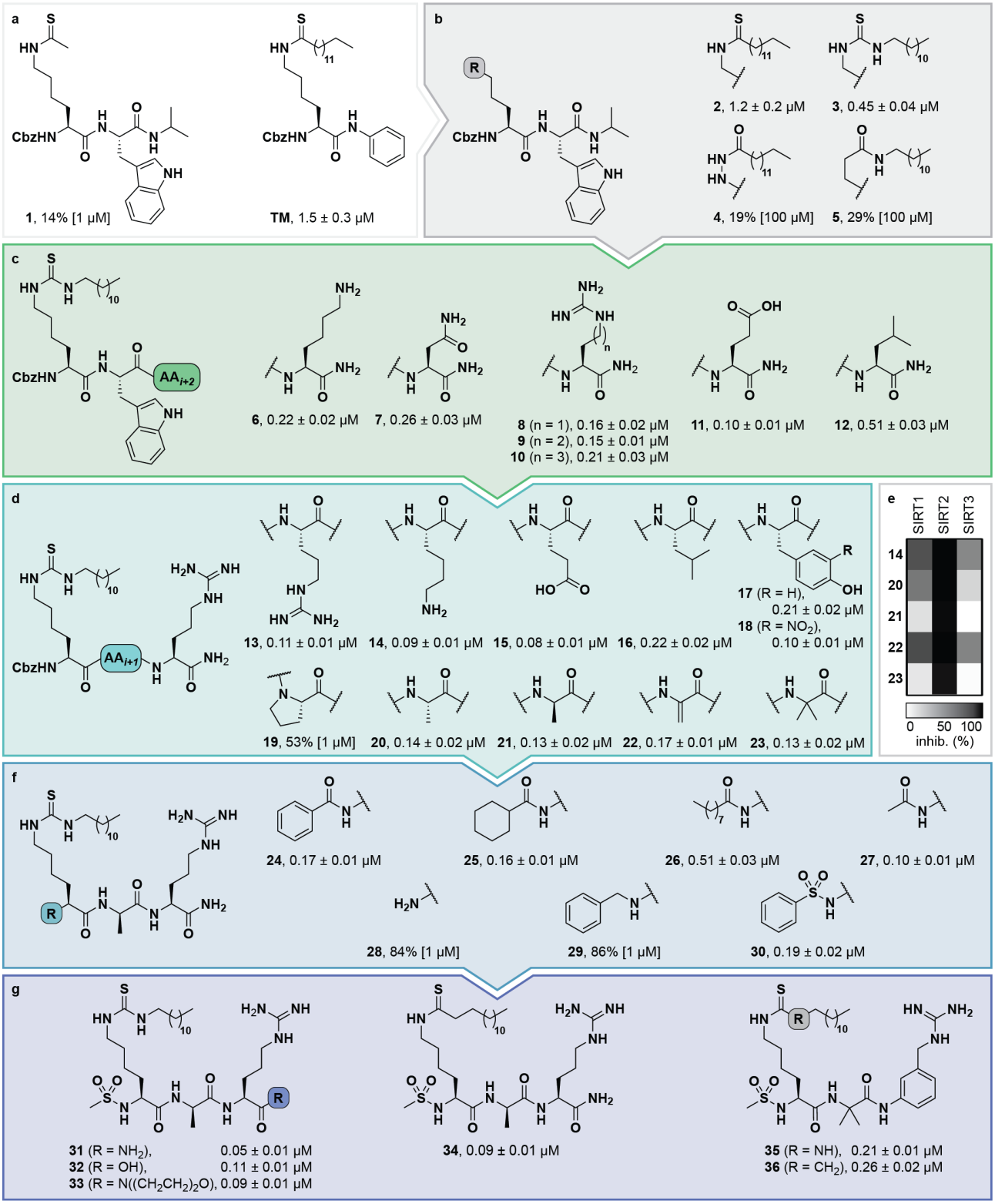

Scheme 1. Structure–activity relationship of SIRT2 inhibitors. Potencies against recombinant SIRT2 are given as mean IC_{50} values ± standard deviation (SD) or %-inhibition. (**a**) Lead compounds. (**b**) Amide isosteres. (**c**) Optimization of position *i*+2. (**d**) Optimization of position *i*+1. (**e**) Heatmap showing %-inhibition against SIRT1–3 of selected compounds at 1 μM. (**f**) Optimization of *N*-terminal group. (**b**) Final inhibitor series. Data are based on two individual experiments performed in duplicate. See the Supplementary Information (Scheme S1, Fig. S1, and Table S1) for dose–response curves and selectivity profiling of additional inhibitors against SIRT1–3.

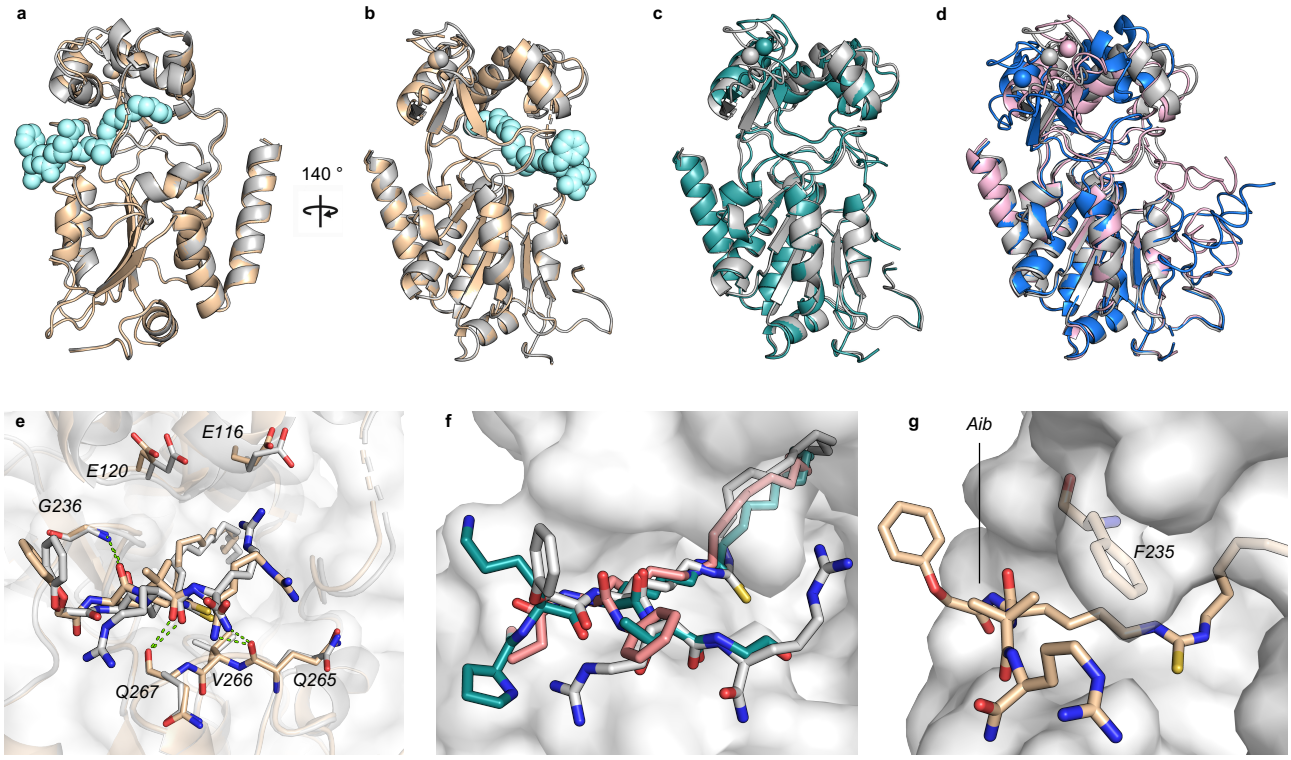

Fig. 2. X-ray co-crystal structures of SIRT2 with compounds 13 and 23 bound. (**a**,**b**) Overall structure of SIRT2 co-crystallized with compounds **13** (gray) or **23** (tan). The ligand (**13**) is shown as light cyan spheres. (**c**) Overlay of the SIRT2:**13** structure (gray) with previously solved co-crystal structure of SIRT2 with the thiomyristoylated peptide substrate analog **BHJH-TM1** (PDB 4R8M; teal). (**d**) Overlay of the SIRT2:**13** structure (gray) with previously solved structure of SIRT2 apo form (PDB 3ZGO; blue) and SIRT2 in complex with **S2iL5** (PDB 4L3O; fuchsia). (**e**) Comparison of the exterior binding pocket of SIRT2 in complex with compound **13** (white) or **23** (tan). Dashed green lines highlight ligand–enzyme hydrogen bonding interactions. (**f**) Surface-view of SIRT2:**13** (white) superimposed with **BHJH-TM1** (teal) and "**glucose-TM**" (PDB 6NR0, pink). (**g**) Surface view of the exterior binding pocket of SIRT2:**23**.

Finally, our structures clearly showed that both L-configured and α-bis-substituted amino acids could be accommodated at the *i*+1 position (Fig. 2e and g) in agreement with our SAR data, including the D-Ala residue at this position. Though, further extension of the side chain of a D-configured residue would likely clash with the nearby F235 of SIRT2 (Fig. 2g). The structures also revealed high flexibility regarding the choice of side chains at both *i*+1 and *i*+2 positions, as no direct interactions with the enzyme were visible. Most prominently, there was a complete lack of electrostatic interactions between the guanidium groups at the *i*+2 position and E120 of SIRT2 (Fig. 2e–g), in contrast to what was observed for **S2iL5**. Again, this observation was in full agreement with the generally subtle differences observed in potency when mutating the *i*+2 position in our SAR. Finally, the structures indicated a significant degree of freedom regarding the choice of *N*-terminal substituents, as also found previously in our optimization of inhibitors of SIRT5.[57]

Based on these considerations, compound **21** was chosen for further optimization by exchange of the *N*-terminal Cbz-group (compounds **24**–**31**, Scheme 1f). The amide-containing derivatives (**24**–**27**) exhibited potency in the same range as **21** with the acetamide (**27**) resulting in the highest potency (IC_{50} = 0.09 ± 0.01 μM), whereas amine-containing compounds **28** and **29** exhibited reduced potency. A sulfonamide group was also well tolerated and the small methanesulfonamide

(**31**) furnished a 4-fold improvement in potency over the more sterically demanding phenylsulfonamide (**30**). Thus, compound **31** is the most potent inhibitor of SIRT2 reported to date and it also shows excellent selectivity for SIRT2 over SIRT1 and SIRT3 (72- and 700-fold, respectively). Nevertheless, we briefly addressed the importance of the *C*-terminal of the inhibitor (Scheme 1g). Applying a synthetic approach using a 2-chlorotrityl resin allowed us to access the *C*-terminal carboxylic acid (**32**), which was also derivatized to give morpholide analog **33**, to explore the effect of additional steric bulk at this position. Both of these compounds exhibited similar excellent inhibitory potency and selectivity. Thus, using the optimized inhibitor **31**, we revisited the importance of the ε-*N*-acyllysine substitution. Reintroducing a thiomyristoyl group furnished compound **34** that could serve as an important tool compound for comparing differences in biological effects between thioamides and thioureas.[64] Truncating the acyl chain decreased the potency dramatically and in a more severe manner than observed for small molecule ligand **TM** and its shorter chain analogs[24] (**S5**–**S6** and **S11**; Scheme S1). Additionally, introduction of oxygen atoms in the acyl chain to increase aqueous solubility greatly decreased the inhibitory activity (**S7**–**S8**, Scheme S1), again emphasizing the importance of a long hydrophobic PTM to maintain binding affinity.

Finally, we synthesized two additional *C*-terminally modified analogs (**35** and **36**), introducing again the Aib moiety in *i*+1 position to circumvent the risk of epimerization during the difficult amide coupling necessary to assemble these compounds with decreased peptide content. These exhibited respectable potency against SIRT2 with only 4–5-fold loss in potency compared to **31**, which may be explained by loss of hydrogen bonding interaction between the *C*-terminal amide group of the *i*+2 residue with Q265 in SIRT2 (Fig. 2e). On the other hand, we reduced the peptidic nature of the compound, which we envisioned could prove beneficial for cell-based experiments.

Inhibition of the deacylase activities of SIRT2. Despite the number of SIRT2 inhibitors previously reported, only few studies have addressed the inhibition of SIRT2 demyristoylase activity.[65,66] However, because K_m values for ε-*N*-myristoyllysine-based substrates are in the order of 100-fold lower than for corresponding acetylated substrates,[6,21] only high-affinity inhibitors should be able to efficiently outcompete myristoylated substrates. Gratifyingly, we found that compound **31** inhibited demyristoylation without enzyme–inhibitor pre-incubation (Fig. 3b), providing support of the hypothesis that high affinity is required for the inhibition of demyristoylation activity. Encouraged by this finding, we sought to emphasize the point further by investigating additional high-affinity binders. We therefore synthesized **S2iL5**[34] (Fig. 1) and its corresponding ε-*N*-dodecylthiocarbamoyllysine analog **37** (**S2iL5^{myr}**, Fig. 3a), which we expected to exhibit even higher potency. Indeed, both compounds showed excellent inhibitory potency comparable to that of compound **31** (Fig. 3c) and we next investigated whether these compounds could also inhibit the demyristoylation activity of SIRT2. Impressively, **S2iL5^{myr}** (**37**) was found to inhibit demyristoylase activity with an IC_{50} value of 110 ± 2 nM while **S2iL5** (2.1 ± 0.2 μM), **31** (9.1 ± 0.8 μM), and **34** (3.3 ± 0.3 μM) were less potent

but still exhibited robust activity without enzyme–inhibitor pre-incubation as opposed to **TM** (Fig. 3b and Table 1).

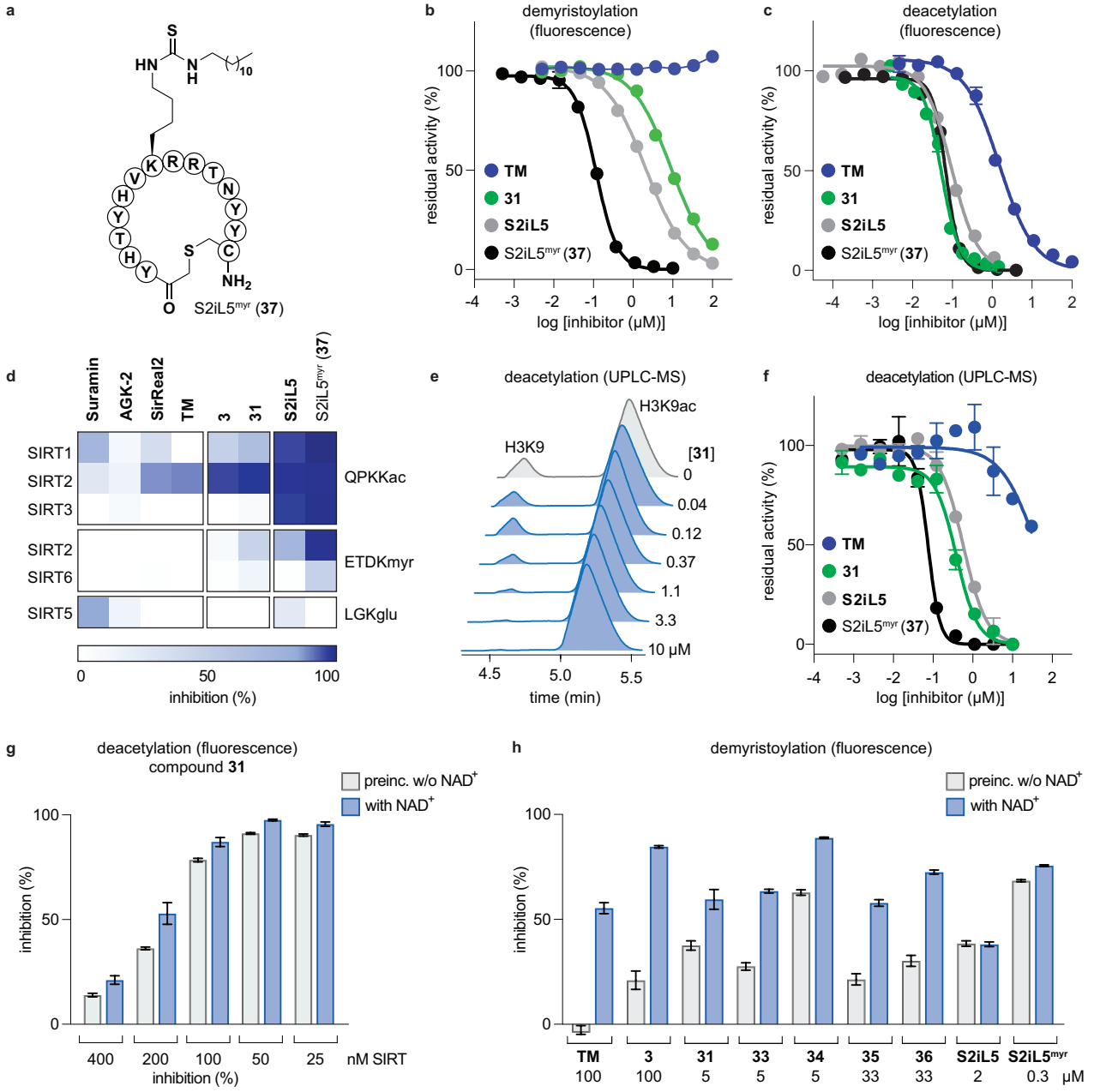

Fig. 3. Sirtuin deacylase activity. (**a**) Structure of **S2iL5**-derived, thiourea-containing macrocycle **S2iL5^{myr}**. (**b**) Concentration–response curves from fluorescence-based *in vitro* sirtuin demyristoylation or (**c**) deacetylation assays. (**d**) Heatmap showing %-inhibition against different sirtuin subtypes at 10 μM (100 μM for SIRT5). See Table S1 and S2 for data. (**e**) HPLC traces (A_{280}) of the hydrolysis of H3K9ac by SIRT2 at varying concentrations of compound **31**. (**f**) Inhibition of SIRT2-mediated deacetylation of H3K9ac determined by LC-MS. (**g**) Pre-incubation experiments, with or without NAD$^+$ (500 μM), of compound **31** (0.10 μM), at variable SIRT2 concentrations. (**h**) Pre-incubation experiments for selected compounds against SIRT2 demyristoylation. Data are based on two individual experiments performed in duplicate. Error bars represent mean ± SEM. See Table S3 for IC_{50} values against SIRT2 mediated H3K9ac deacetylation.

Table 1. IC_{50} values (μM) or %-inhibition data for final compounds and control compounds*

compound	SIRT1	SIRT2		SIRT3	cLogP†	PSA† (Å^2)
	AMC^{Kac}	AMC^{Kac}	AMC^{Kmyr}	AMC^{Kac}		
SirReal2	37% [10 μM]	0.91 ± 0.08	n.a.§	n.a.	5.14	72.0
TM	n.a.	1.5 ± 0.3	n.a.	n.a.	8.62	96.4
tenovin-6	<50% [100 μM]	19 ± 1	n.a.	<50% [100 μM]	5.39	98.5
AGK-2	62% [100 μM]	50 ± 10	n.a.	69% [100 μM]	5.08	77.5
S2iL5	0.24 ± 0.03	0.09 ± 0.01	2.1 ± 0.2	0.30 ± 0.03	–	–
S2iL5^{myr}	0.14 ± 0.03	0.07 ± 0.01	0.11 ± 0.02	0.18 ± 0.02	–	–
31	3.6 ± 0.7	0.05 ± 0.01	9.1 ± 0.8	35 ± 3	1.90	264
33	4.8 ± 0.8	0.09 ± 0.01	13 ± 2	55 ± 5	2.67	247
34	3.7 ± 0.2	0.09 ± 0.01	3.3 ± 0.3	<50% [10 μM]	2.52	255
35	14 ± 2	0.21 ± 0.01	93 ± 7	n.a.	4.92	206
36	14 ± 1	0.26 ± 0.02	84 ± 8	<50% [10 μM]	5.39	201

*All values represent the mean of at least two individual assays performed in duplicate and are given in μM ± SD. These assays were performed under standard conditions without pre-incubation.[67]
†cLogP and polar surface area (PSA) values were calculated using QikProp.[68]
§n.a. = no activity, denotes no measurable inhibition above control wells at 10 μM inhibitor concentration.

Our novel compounds were then benchmarked on potency against the deacetylation activity of SIRT2 and selectivity over other sirtuin enzymes, by applying a series of control compounds found in literature (Fig. 3c,d and Table 1). Within this series, all our novel compounds **31** and **33**–**36** showed superior potency compared to **SirReal2**, **AGK-2**, **tenovin-6**, **suramin**, and **TM**. The macrocycle **S2iL5** and its long-chain acylated homolog **37** were equipotent to our novel inhibitors but also potently inhibited both SIRT1 and SIRT3 to exhibit a lower degree of selectivity (Fig. 3d, Fig. S2, and Table 1). We also calculated the cLogP and polar surface area (PSA) values for novel inhibitors and control compounds (Table 1). For the cLogP values, our compounds were approximately 5 or lower, which is comparable to **SirReal2**, **AGK-2**, and **tenovin-6**, while **TM** was substantially higher at 8.6. For the PSA, our compounds were generally higher than control compounds, but encouragingly, substituting the *C*-terminal amino acid with *meta*-aminobenzylamine (compounds **35** and **36**) led to a 20% decrease in PSA. Thus, theoretically improving the cell permeability compared to the compounds with higher peptide content (**31**, **33**, and **34**). On the other hand, the generally higher PSA values for our compounds compared to the small molecule control compounds also gives rise to better aqueous solubility enabling biological studies without the need for drug formulation.

Next, we investigated whether the observed inhibition of enzymatic deacylation was related to direct interactions with the substrate AMC fluorophore.[69] To address this, we chose a label-free HPLC-MS-based assay, monitoring inhibition of H3K9ac deacetylation (Fig. 3e,f). We found the potencies of compounds **31**, **S2iL5**, and **S2iL5^{myr}** to be recapitulated, exhibiting IC_{50} values in the sub-micromolar range. Interestingly, **TM** showed more than 100-fold lower potency than **31** (IC_{50} ~40 μM and 0.39 ± 0.08 μM, respectively) when tested on histone peptide and analyzed by UPLC-MS. This is not in accordance with a recent study by Lin[66] but corresponds well with another report where **TM** is

used as a reference compound.[65] Thus, *in vitro* IC_{50} values are highly dependent on the experimental conditions applied and calls for a more standardized measurement of compound potencies and/or determination in several different assay formats.[70] Additionally, simple dose–response competition assays (*i.e.* without enzyme–inhibitor pre-incubation) do not take into account the kinetic behavior of inhibitors, which may give rise to somewhat arbitrary IC_{50} values; especially, if the compound does not exhibit standard fast-on/fast-off kinetics.[13,57,71] It is well documented that mechanism-based thioamide- and thiourea-containing inhibitors may form stalled intermediates between substrates and ADPR in the enzyme active sites, which can affect binding kinetics.[72] We therefore attempted to obtain additional kinetic insight by performing continuous assays.[57,73] This format was unfortunately found unsuitable due to too rapid degradation of SIRT2 under the experimental conditions (Fig. S3). Instead, we performed pre-incubation experiments with selected inhibitors and SIRT2 with or without addition of NAD^+ to address whether the inhibitors exhibited slow-binding. For early inhibitors in the SAR study (**2**, **3**, and **TM**), we observed an increase in %-inhibition upon pre-incubation in the presence of NAD^+, suggesting that binding involves the formation of stalled intermediates (Fig. S4).[57] For thioacetylated compounds **S1**–**S4** the opposite effect was observed (Fig. S4a), which is presumably due to cleavage of the thioacetamide groups as recently described.[64] The effect of pre-incubation was also reduced when inhibitor potencies increased and approached stoichiometric inhibitor–enzyme levels (Fig. 3g and Fig. S4). On the other hand, substantial increase in %-inhibition values were recorded upon pre-incubation including NAD^+ when attempting to inhibit demyristoylation, except with compounds **S2iL5** and **S2iL5^{myr}** (Fig. 3h).

Compound stability. Over the last decade, the considerable efforts in development of efficacious sirtuin modulators has furnished a number of potent inhibitors of commercial interest of which some have entered clinical trials to document safety and efficacy in humans.[74–79] However, there is a lack of studies addressing the chemical- and metabolic stability of sirtuin inhibitors, except for one study of pronase susceptibility of linear vs. cyclic sirtuin inhibitors.[80] We recently addressed how stability differed greatly between short chain thioamide and thiourea compounds,[64] which prompted us to investigate stability of selected inhibitors developed in this study. We first addressed the stability of **31** (thiourea) and **34** (thioamide) in buffer and both compounds remained intact under the *in vitro* assay conditions for up to 10 days at 37 °C (Fig. S13). Next, we investigated the stability in human serum, which, in agreement with our previous observations,[64] revealed that compound half-lives ($t_{½}$) of thioamides (**TM**, **2**, **34**, and **36**) were significantly higher than their thiourea counterparts (**3**, **31**, and **35**), with the latter series being almost fully degraded in less than two hours (Fig. 4a). Additionally, we measured the stability of three known SIRT2 inhibitors for comparison. The **tenovin-6** and **S2iL5** were rapidly degraded whereas the small molecule inhibitor **SirReal2** exhibited superior stability with no degradation even after 24 h (Fig. S14c).

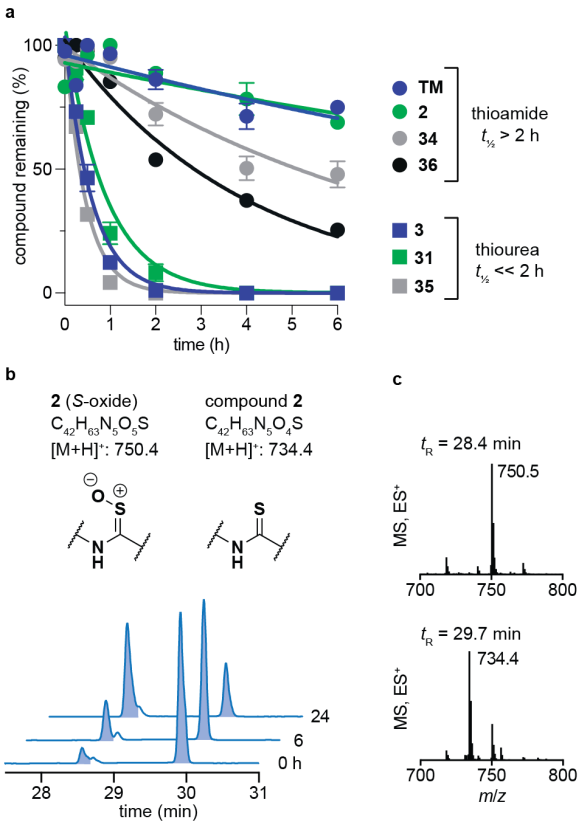

Fig. 4. Stability assays in human serum. (**a**) Stability assays of selected compounds in human male serum. (**b**) UV (A_{280}) and (**c**) TIC (ES) chromatograms and mass spectra at relevant time points of compound **2** monitoring degradation in serum. Data are shown as mean values relative to the peak intensity at t = 0 h ± SEM, n = 2–3. For $t_{½}$ values, see Table S4.

The degradation of compounds **2** (thioamide) and **3** (thiourea) could be scrutinized in more detail by UPLC-MS analysis because they contain tryptophan as a suitable chromophore. We found that the thioamide (**2**) was converted to a species with $[M+16]^+$ (m/z) to a significant extent (Fig. 4b). Because thioamide *S*-oxides are known oxidative metabolites, we hypothesized that this is the major degradation product (Fig. 4b).[81,82] The rapid degradation of the corresponding thiourea (**3**), on the other hand, led to large number of species that could not be structurally determined (Fig. S15). Release of hydrogen sulfide from both thioamide and thiourea motifs constitutes another possible mechanism of degradation.[83] These results suggest that enzymes other than peptidases (*i.e.* redox active enzymes) may play a significant role in compound turnover, which raises the question whether these compounds will stay intact *in vivo*. Due to detrimental effects of serum on stability, we also tested whether both thioamide- and thiourea-containing compounds remained stable in cell growth medium supplemented with fetal bovine serum (FBS). Gratifyingly, no degradation was observed for compounds **31** and **34** after 24 h, rendering both amenable as probes for cell culture experiments (Fig. S14a).

Effect of SIRT2 inhibition on α-tubulin acetylation. With our series of potent inhibitors in hand, we then assessed the cytotoxicity of a selection of 15 compounds in cell culture experiments. We

chose a panel of four cell lines, including immortalized human epithelial kidney cells (HEK293), solid cervical cancer cells (HeLa), breast cancer cells (MCF-7), and T lymphocytes (Jurkat). Despite strong potency against SIRT2 *in vitro*, the compounds displayed low cytotoxicity, particularly against the breast cancer cell line MCF-7, whereas Jurkat cells were more susceptible (Fig. S5 and Table S5). Interestingly, the "rigidified" compounds **35** and **36** were significantly more cytotoxic with GI_{50} values down to 3 μM, which may reflect better cell permeability than compounds **31** and **34**. But dedicated investigations are required to unambiguously show this.

To investigate whether the compounds affected the protein acetylation level in cells, we incubated HeLa and MCF-7 cells under a series of conditions and performed Western blots on cell lysates to monitor changes in acetylation levels of α-tubulin, which is a known target of SIRT2.[16] Disappointingly, we failed to see any reproducible changes in acetylation levels upon treatment with inhibitor, including **TM** as the positive control,[24] and this was the case even upon overexpression of SIRT2 or inhibition of HDAC6, which also targets α-tubulin, by co-treatment with trichostatin A (**TSA**)[47] (Fig. S6–S12). Interestingly, we found that despite increasing the cellular levels of SIRT2 upon overexpression, the levels of Ac-α-tubulin were unaltered, thereby questioning the effect of SIRT2 on global deacetylation of α-tubulin in both HeLa and MCF-7 cells. Part of the explanation for this observation may be the differences in acetylation in asynchronous and mitotic cells.[17]

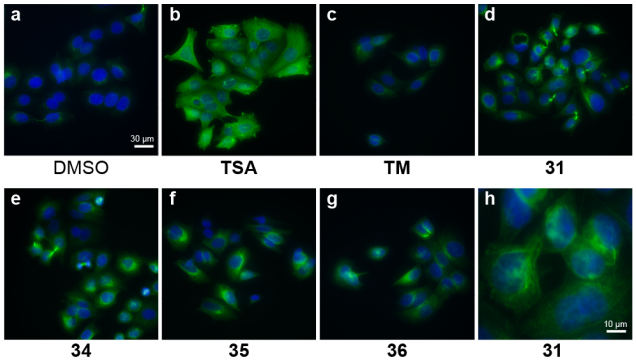

Fig. 5. SIRT2 inhibition affects perinuclear α-tubulin acetylation. (**a**–**g**) Immunofluorescence images (40×) of MCF-7 cells subjected to 6 h treatment with inhibitor (25 μM, 5 μM for TSA) or DMSO (vehicle). (**h**) Zoomed image for compound **3**. DAPI (blue, nuclear counterstain) and Ac-α-tubulin (green). For additional images (single-filtered and zoomed), please see Fig. S16. The data are representative images from two individual experiments.

Instead, we used immunofluorescence as a readout to detect changes in acetylated α-tubulin levels in MCF-7 cells. Upon treatment with inhibitor (25 μM for 6 hours), we were pleased to observe an increase in cellular fluorescence levels, particularly around the perinuclear microtubules,[35] which is reported to be the main target of SIRT2 inhibition in cells.[84] Treatment with the potent HDAC6 inhibitor **TSA**, on the other hand, resulted in hyperacetylation of α-tubulin throughout the entire cell (Fig. 5). Conclusively, the SIRT2 mediated effects on α-tubulin acetylation is mainly perinuclear compared to the global effects mediated by HDAC6 deacetylation,[84] which helps explain why

Western blotting of the global levels of Ac-α-tubulin is not an ideal measure of the effect of SIRT2 inhibition, knockdown, or overexpression in cells.

Inhibition of SIRT2 reduces breast cancer cell motility. Due to the effects of our compounds on the acylation of the cytoskeleton, we next investigated the role of SIRT2 inhibition on breast cancer cell motility. In previous reports, SIRT2 has been implicated in the migration and invasion of gastric, colon, lung, and liver cancers.[85–88] Therefore we wanted to investigate the effect on cell motility when inhibiting SIRT2 in MCF-7 cells. We first investigated the effects of selected inhibitors in a scratch assay (wound-healing assay) and all inhibitors decreased the degree of migration compared to the vehicle-treated control at non-cytotoxic concentrations (Fig. 6a,b and Fig. S18). We further investigated compound **34** in more detail by performing migration and invasion assays. Upon 24 h treatment, we observed a reduction in migration by approximately 30%, while cell invasion through Matrigel-coated inserts was drastically decreased by 84% (Fig. 6c,d). Interestingly, the even greater effect on cell invasion could suggest that SIRT2 plays a critical role in tumor metastasis in breast cancer although additional studies are required to confirm this. Interestingly, knockdown of SIRT2 was recently shown to have the opposite effect on migration of A549 cells overexpressing RalB in culture,[88] indicating that pharmacological modulation of the SIRT2 activity may provide a different outcome from enzyme knockdown/overexpression or that the effects are cell type specific.

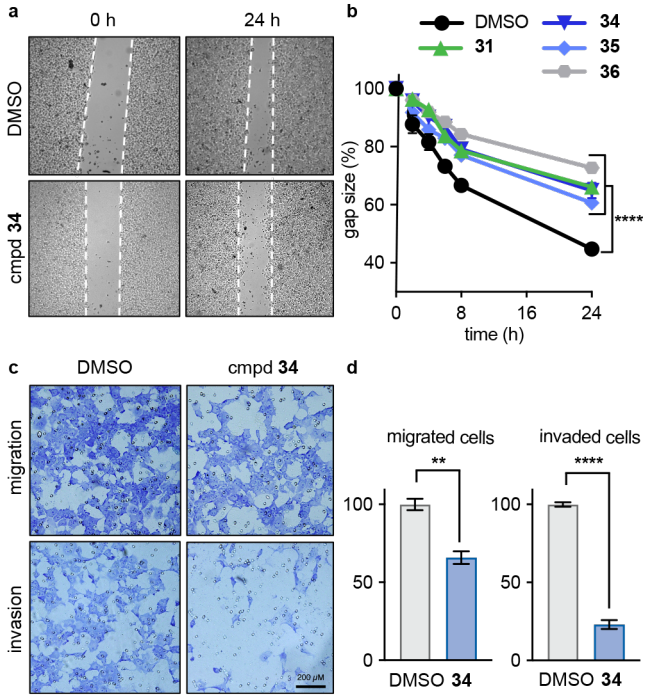

Fig. 6. SIRT2 inhibition elicits decreased breast cancer cell motility. (**a**) Representative images from a scratch assay in MCF-7 cells at time points 0 and 24 h (2.5× magnification). For images from scratch assays for additional compounds, see Fig. S17. (**b**) Quantification of the gap size at different time points treated with inhibitors (**31** and **34**, 25 μM; **35** and **36**, 10 μM) relative to control (1% DMSO) treated cells ± SEM (**c**) Representative Boyden assay images of migrated and invaded MCF-7 cells. (**d**) Quantification of migrated and invaded cells upon treatment with compound **34** (25 μM) over 24 h. Data are shown as mean values relative to control (1% DMSO) treated cells ± SEM, n = 3-4; ***P* < 0.01; *****P* < 0.0001. Statistical differences from control treated cells were determined by unpaired parametric t-tests.

Discussion

Here we report an extensive SAR study, including X-ray cocrystal structures with intermediary inhibitors bound to SIRT2 to provide structural rationalization of the optimization of binding potency. This furnished the most potent inhibitors of the SIRT2 histone deacetylase enzyme reported to date, which at the same time exhibit excellent selectivity for the target compared to its structurally similar isoforms, SIRT1 and SIRT3 (>50-fold). Also, the compounds were able to inhibit the demyristoylase activity of SIRT2, which is far more challenging due to the low K_m values of Kmyr-containing substrates. We furthermore provide insight into the binding kinetics of the SIRT2 inhibition as well as measures of stability in buffer, cell culture medium, and human serum, which taken together will inform the development of future generations of mechanism-based inhibitors of sirtuins in general.

We show that slow-binding kinetics – and hence an effect of pre-incubation on IC_{50} value in enzymatic assays – becomes negligible when the compound affinity increases. This was particularly evident for the inhibition of SIRT2 demyristoylase activity of the peptide macrocycles. Whereas, potent inhibition of demyristoylase activity of lead compounds **34** and **36** were relying more strongly on enzyme–inhibitor preincubation. Due to the effects of assay conditions on IC_{50} values, the collective data also show that more standardized protocols should be pursued and that potencies should ideally be determined in more than one assay format. To our satisfaction, trends in compound potencies determined in our standard fluorescence-based were indeed reflected when applying an alternative HPLC-MS-based assay for selected compounds.

The thiourea-containing compounds are more readily synthesized than thioamide counterparts but proved significantly less stable in human serum, highlighting probes **34** and **36** as the preferred choices for biological applications. Due to the similar potencies of inhibitors containing these two functional groups, however, we still find the thiourea-based compounds useful during SAR studies, focusing on the optimization of compound potency and selectivity *in vitro*. At a later stage, the resulting lead compounds can then be prepared as their thioamide counterparts for biological studies as demonstrated in this work.

Satisfyingly, all members of our final compound series **31** and **34**–**36** demonstrated cellular activity by causing increased levels of perinuclear acetylated α-tubulin in MCF-7 cells in culture. This was revealed by immunofluorescence experiments while Western blot analyses failed to demonstrate a statistically significant effect in a range of experiments, including overexpression and/or treatment with additional HDAC inhibitors. Our data, together with previously published reports,[35,84] therefore strongly suggest that Western blotting of global Ac-α-tubulin levels should not be applied for determining modulation of the SIRT2 activity in cells. Finally, we show that both migration and invasion of cultured MCF-7 cells is reduced by our SIRT2 inhibitors, which could have implications for inhibiting cancer metastasis.

Taking a different approach, Liu and co-workers discovered equally potent peptide-based, mechanism-enabled inhibitors of SIRT2 in a report published while the current contribution was in

final preparation.[89] In their report, a powerful amber-obligate phage display technology was developed and applied to the discovery of potent and selective inhibitors of SIRT2. This also provided consensus sequence data from screening of large libraries, which could be useful for additional future fine tuning of ligand potency. However, the hit sequences were peptide heptamers, which would likely be vulnerable to protease activity and have limited cell permeability. Also, no demonstration of cellular activity was provided as the focus of the study was demonstration of the power of the developed amber-obligate phage library technology and not probe compound development.[89]

Thus, the probes reported herein provide an attractive alternative to previously developed SIRT2 inhibitors by exhibiting potent and selective inhibition of SIRT2, including both the ability to inhibit its deacetylase and demyristoylase activities. Furthermore, the compounds exhibit activity in cells, stability in serum, and aqueous solubility that should allow for *i.v.* dosing of animals without elaborate drug formulation. This combination of features is unique among SIRT2 inhibitors and we expect that the developed probes will therefore be valuable in the continued investigation of the function of SIRT2 as well as the development of novel therapeutics that target this enzyme.

Methods

For general experimental information, chemical synthesis, compound characterization data, additional methods, and copies of ^{1}H, ^{13}C, and ^{19}F NMR spectra of novel compounds, please consult the Supplementary Information.

Materials and methods for the biochemical assays. SIRT1 (aa 193–741 with *N*-terminal GST-tag, ≥60% purity; cat. #50012), SIRT2 (aa 50–356 with *C*-terminal His-tag, ≥90% purity; cat. #50013), SIRT3 (aa 102–399 with *N*-terminal GST-tag; ≥64% purity; cat. #50014), and SIRT6 (full length with *N*-terminal GST-tag, ≥75% purity; cat. #50017) were from BPS Biosciences (San Diego, CA). SIRT5 (aa 37–310 with *N*-terminal His-tag, ≥95% purity; cat. #BML-SE555-0050) was purchased from Enzo Life Sciences (Farmingdale, NY). Purities were based on SDS-PAGE and Coomassie blue stain according to the supplier and all enzyme concentrations given were based on the stock concentrations determined by the supplier. Sirtuin substrates were obtained from previous studies: Ac-Gln-Pro-Lys-Lys(Ac)-AMC (QPKKac),[20] Ac-Glu-Thr-Asp-Lys(Ac)-AMC (ETDKac),[21] Ac-Glu-Thr-Asp-Lys(Myr)-AMC (ETDKmyr),[90] Ac-Lys-Gln-Thr-Ala-Arg-Lys(Ac)-Ser-Thr-Gly-Gly-Trp-Trp-NH_2 (H3K9ac),[20] and Ac-Leu-Gly-Lys(Suc)-AMC (LGKsuc).[9] Assay buffer was prepared as described in Biomol International product sheets (BML-KI-143; Tris HCl (50 mM), NaCl (137 mM), KCl (2.7 mM), $MgCl_2$ (1 mM), pH 8.0) with addition of BSA (1.0 mg/mL, Sigma; cat. #A2153) unless stated otherwise. Trypsin (10,000 units/mg, TPCK treated from bovine pancreas; cat. #T1426) was purchased from Sigma (Steinheim, Germany). All other chemicals and solvents were of analytical grade and were used as obtained from commercial suppliers without further purification. All reactions were performed in black low binding 96-well microtiter plates (Corning half area wells), with duplicate

series in each assay and each assay performed at least twice. All reactions were performed in assay buffer, with appropriate concentrations of substrates and inhibitors obtained by dilution from 2–50 mM stock solutions in either water or DMSO. The DMSO concentration in the final assay solution did not exceed 1% (v/v) and control wells without either enzyme (negative control) or inhibitor (positive control) were included in each plate. Plates were analyzed using either a Perkin Elmer Enspire or a BMG Labtech FLUOstar Omega plate reader with excitation at 360 nm and detecting emission at 460 nm. Fluorescence measurements (RFU) were converted to [AMC] concentrations based on an [AMC]-fluorescence standard curve, and all data analysis was performed using GraphPad Prism (version 8.1.2).

End-point SIRT inhibition assays. End-point inhibition assays were performed as previously described.[57] In brief, the relevant substrate, NAD^+ (Sigma; cat. #N5755), and inhibitor were added to each well and the experiment was initiated by addition of a freshly prepared solution of relevant sirtuin, for a final volume of 25 μL per well. The following final concentrations were used: SIRT enzyme (100 nM; 600 nM for SIRT6), substrate (50 μM), NAD^+ (500 μM), and inhibitor (1, 10, or 100 μM or 2- or 3-fold dilution series for dose–response assays). The plate was incubated at 37 °C for 60 min, then a solution of trypsin and NAM (25 μL, 5 mg/mL and 4 mM, respectively; final concentration 2.5 mg/mL and 2 mM, respectively) was added and the assay development was allowed to proceed for 90 min at RT, before fluorescence measurement and calculation of residual activity. For concentration-response assays, IC_{50} values were obtained by fitting the resulting data to the concentration–response equation using GraphPad Prism (version 8.1.2).

Continuous enzyme inhibition assays. Rate experiments for determination of kinetic parameters were evaluated under varying inhibitor concentrations.[67] Buffer was prepared as previously described[21] [50 mM HEPES/Na, pH 7.4, 100 mM KCl, 0.01% Tween-20, 0.2 mM TCEP, BSA (0.05 mg/mL]. SIRT2 was incubated with the relevant substrate, inhibitor and trypsin in assay buffer in a total volume of 50 μL per well using the following final concentrations: SIRT2 (500 nM); ETDKac (150 μM), inhibitor (100–0.03 μM; 2.5 fold dilution series), NAD^+ (500 μM) and trypsin (40 ng/μL). *In situ* fluorophore release was monitored immediately by fluorescence readings recorded every 30 seconds for 20 min at RT.

End-point pre-incubation assays. SIRT1/2 and inhibitor was pre-incubated with or without NAD^+ for 30 min at 37 °C in a total volume of 40 μL, prior to addition of substrate (and NAD^+ if excluded in pre-incubation), for a final volume of 45 μL. For pre-incubation excluding NAD^+, the following concentrations were used: SIRT1/2 (113 nM during pre-incubation, giving 100 nM after substrate and NAD^+ addition), inhibitor (ranging from 113/100 μM down to 0.07/0.06 μM), substrate (0/50 μM) and NAD^+ (0/500 μM); For pre-incubation including NAD^+, the following concentrations were used: SIRT2 (113 nM during pre-incubation, giving 100 nM after substrate and NAD^+ addition), inhibitor (ranging from 113/100 μM down to 0.07/0.06 μM), substrate (0/50 μM) and NAD^+ (563/500 μM). The

plate was incubated at 37 °C for 30 min, then a solution of trypsin and nicotinamide (45 μL, 5.0 mg/mL and 4 mM, respectively; final concentration 2.5 mg/mL and 2 mM, respectively) was added and the assay development was allowed to proceed for 90 min at RT, before fluorescence measurement and calculation of residual activity.

End-point enzyme stoichiometry assays. Using the protocol described above, the following concentrations were used after addition of substrate. SIRT2 (400–25 nM; 2-fold dilutions) after addition of substrate), inhibitor (compound **31**; 0.10 μM), QPKKac (50 μM) and NAD^+ (500 μM). The plate was incubated at 37 °C for 60 min, then a solution of trypsin and nicotinamide (45 μL, 5.0 mg/mL and 4 mM, respectively; final concentration 2.5 mg/mL and 2 mM, respectively) was added and the assay development was allowed to proceed for 90 min at RT, before fluorescence measurement and calculation of residual activity.

HPLC-MS-based SIRT inhibition assays. All reactions were performed in black low binding 96-well microtiter plates (Corning half-area wells), with each assay performed twice, using the same assay buffer as in the fluorescence-based assays, but with the omission of BSA. Inhibition assays (concentration–response) were performed in a final volume of 80 μL/well. The following final concentrations were used: SIRT2 (20 nM), inhibitor (3-fold dilution series), H3K9ac (50 μM) and NAD^+ (500 μM). After incubating SIRT2, substrate, and inhibitor (when applicable) for 30 min at 37 °C, the reaction mixture was quenched by the addition of ice-cold MeOH/HCOOH (96:4 (v/v), 20 μL). The samples were analyzed by UPLC-MS on a Waters Acquity ultraHPLC-MS system equipped with a diode array detector. A gradient with eluent I (0.1% HCOOH in water (v/v)) and eluent II (0.1% HCOOH in MeCN (v/v)) rising linearly 0–10% during *t* 0.00–2.00 min followed by 10–30% of eluent II during *t* 2.00–7.00 min was applied at a flow rate of 0.6 mL/min. The obtained chromatograms at 280 nm were used to determine reaction progression, by determining area under the curve of the relevant peaks using Waters MassLynx.

Chemical stability assays. *Serum stability:* 400 μL human male serum (Sigma; cat. #H4522) was incubated at 37 °C for 15 min. The serum was spiked with a DMSO-stock solution of the respective inhibitor to reach a final concentration of 150 μM. The mixture was shaken at 750 rpm in an incubator at 37 °C. Samples (45 μL) were taken out at time points (0 min, 15 min, 30 min, 1 h, 2 h, 4 h, 6 h, and 24 h) and quenched with aqueous urea (6 M, 50 μL) and incubated for 10 min at 4 °C. Ice-cold acetonitrile (100 μL) was added to the sample and incubated for another 10 min at 4 °C. The samples were centrifuged for 90 min at 20,000 g and filtered (0.50 μm) before analysis by HPLC and subsequent integration of the peak areas of recovered compound over time. Half-lives ($t_{½}$) were determined using GraphPad Prism (version 8.1.2) and fitted to a one-exponential decay equation, assuming first-order kinetics. Each assay was performed at least twice.

Cell-media stability: For compounds **31** and **34**, a similar procedure to the above described was performed using MEM cell-medium (Sigma; cat. #2279) containing FBS (10% (v/v)).

Buffer stability: A DMSO-stock solution of compound **20**, **31**, or **34** was diluted to a final concentration of 100 μM in SIRT buffer (Tris buffer, pH 8.0). The mixture was shaken at 750 rpm in an incubator at 37 °C and samples were taken out at time points (0, 2, 5, and 10 days) and analyzed on a UPLC system.

Immunocytochemistry. MCF-7 cells (150 cells/well) were plated in Labtek Permanox Plastic Chamber slide system (Nunc, Thermo Scientific; cat. #177445) and incubated overnight. After 24 h, the cells were treated with inhibitor at the noted concentration or DMSO (control) for 6 h, after which the cells were fixed in 4% formaldehyde for 15 min at RT. Cells were rinsed three times with PBS (pH 7.4) before blocking for 1 h with blocking buffer [5% goat-serum in PBST (PBS + 0.1% Triton-x100)] at RT and were then incubated with acetylated α-tubulin antibody (1:300, Santa Cruz Biotechnology, Dallas, TX; cat. #sc-23950 AC) in 5% goat-serum in PBST overnight at 4 ˚C. The cells were washed in PBS three times and the fluorophore conjugated antibody diluted in blocking buffer (goat-anti mouse Alexa 488, Thermo Fisher, Waltham, MA; cat #A11011) was added 1:800 and incubated 1 h in the dark at RT. After three washes with PBS, the slides were mounted using ProLong® gold antifade mountant with DAPI (Thermo Fisher; cat. #P36941) and cells were visualized using an inverted fluorescence microscope at 40×. Images were generated using Visiopharm technology (Visiopharm, Hørsholm, DK), processed using ImageJ (version 1.8) and Adobe Photoshop Lightroom (version 5.3).

Scratch assays. MCF-7 cells were plated in ibidi 2-well culture inserts (Ibidi Gmbh, Gräfelfing, Germany; cat. #80209) in 24-well plates at 300,000 cells/well and incubated overnight. After overnight incubation, the inserts were removed and the cells were washed once in PBS and fresh medium was added. Cells were left to settle for 15 min before adding culture medium containing SIRT2 inhibitor (25 μM for **31** and **34**; 10 μM for **35** and **36**) or a DMSO control. Brightfield images were taken at time points 0, 2, 4, 6, 8, and 24 h and the gap areas for each image were calculated using ImageJ (version 1.8) and used to determine the %-closure of the gaps at each time point.

Cell migration/invasion assays. Cell migration and invasion assays were performed using 24-well porous (8 μm) Transwell inserts (Falcon, Corning, NY) – coated with diluted Matrigel for invasion assays – according to manufacturer's recommendations. MCF-7 cells were suspended in serum-free media (0.1 mL, MEM, 1% penicillin-streptomycin, 1% glutamine, 1% non-essential amino acids, 0.2% FBS) with *or* without SIRT2 inhibitor **34**, and 10,000 cells were seeded onto the upper part of the cell insert. Culture medium including 10% FBS as chemoattractant was added to the lower chambers and the chamber was incubated at 37 °C in an atmosphere containing 5% CO_2 and 95% humidity for 24 h. The non-migrating or non-invaded cells were gently removed by scrubbing with a cotton swab and the migrated/invaded cells located on the opposite site of the cell insert were fixed with 100% MeOH and stained with Differential Quik III Stain (Polysciences Inc., Warrington, PA; cat. #26419). Five random fields of view per membrane were generated using VIS (Visiopharm,

Hørsholm, Denmark). The data is reported as the average number of migrated cells compared to the control group (control set to a 100% migration or 100% invasion).

Crystallization and X-ray co-crystal structures. Crystallization was obtained using the catalytic domain of human SIRT2 lacking loop regions comprising 292–303: residues (52–291) + (304–356). The SIRT2 catalytic domain (16 mg/mL) and compound **13** or **23** (final concentration 1 mM) were mixed, and crystallization screening was performed using commercial kits (Hampton Research, Aliso Viejo, CA). Crystals for X-ray crystallography were obtained using 0.1 M HEPES, pH 7.0, 30% (v/v) with Jeffamine ED-2001, pH 7.0 for compound **13** or with 0.15 M potassium bromide, 30% (w/v) polyethylene glycol monomethyl ether 2,000 for compound **23** at 20 °C. Crystals were frozen with liquid nitrogen using PEG400 10% (w/v) as cryoprotectant. X-ray diffraction data were collected at 100 K in a nitrogen gas stream at the synchrotron beamlines, PF-BL 5A, 17A at Photon Factory and X06DA at the Swiss Light Source. Data were processed and scaled with the XDS program package.[91] The crystal structures were determined by the molecular replacement method with MOLREP,[92,93] using the structure of SIRT2 in complex with H3K9-myr peptide (PDB 4Y6L).[51] Refinement and model building were performed with REFMAC5[93,94] and Coot.[95] Coordinates of inhibitors were calculated in AceDRG.[96] The geometric quality of the model was assessed with MolProbity.[97] Data collection and refinement statistics are listed in Table S6. Structure figures were created with PyMOL Molecular Graphics System (version 1.8.0.6., Schrödinger, LLC).

Abbreviations

ADPR, adenosine diphosphate ribose; Aib, 2-aminoisobutyric acid; AMC, 7-amino-4-methylcoumarin; BSA, bovine serum albumin; Cbz, benzyloxycarbonyl; DAPI, 4',6'-diamidino-2-phenylindole; DMSO, dimethylsulfoxid; ES, electrospray; FBS, fetal bovine serum; HDAC, histone deacetylase; HEK293, human embryonic kidney 293 cells; HeLa, Henrietta Lacks (human cervical cancer cells); HEPES, (4-(2-hydroxyethyl)-1-piperazineethanesulfonic acid); GFP, green fluorescent protein; GI_{50}, half growth inhibitory concentration; HPLC, high-performance liquid chromatography; IC_{50}, half maximal inhibitory concentration; *i.v.*, intravenous; LC, liquid chromatography; MCF-7, Michigan cancer foundation; MEM, minimum essential medium eagle; NAD, nicotinamide adenine dinucleotide; NAM, nicotinamide; NMR, nuclear magnetic resonance; PBS, phosphate-buffered saline; PDB, Protein Data Bank; PSA, polar surface area; PTM, post-translational modification; RT, room temperature; SAR, structure-activity relationship; SD, standard deviation; SEM, standard error of the mean; SIRT, sirtuin; SPPS, solid-phase peptide synthesis; TIC; total ion chromatogram; TSA, trichostatin A; UPLC, ultra-high performance liquid chromatography.

References

1. Bheda, P., Jing, H., Wolberger, C. & Lin, H. The substrate specificity of sirtuins. *Annu. Rev. Biochem.* **85**, 405–429 (2016).
2. Rajabi, N., Galleano, I., Madsen, A. S. & Olsen, C. A. Targeting sirtuins: Substrate specificity and inhibitor design. in *Prog. Mol. Biol .Transl. Sci.* **154**, 25–69 (Academic Press, 2018).
3. Du, J. *et al.* SIRT5 is a NAD-dependent protein lysine demalonylase and desuccinylase. *Science* **334**, 806–809 (2011).
4. Jiang, H. *et al.* SIRT6 regulates TNF-α secretion through hydrolysis of long-chain fatty acyl lysine. *Nature* **496**, 110–113 (2013).
5. Feldman, J. L., Baeza, J. & Denu, J. M. Activation of the protein deacetylase SIRT6 by long-chain fatty acids and widespread deacylation by mammalian sirtuins. *J. Biol. Chem.* **288**, 31350–31356 (2013).
6. Teng, Y. Bin *et al.* Efficient demyristoylase activity of SIRT2 revealed by kinetic and structural studies. *Sci. Rep.* **5**, 8529 (2014).
7. Tan, M. *et al.* Lysine glutarylation is a protein posttranslational modification regulated by SIRT5. *Cell Metab.* **19**, 605–617 (2014).
8. Mathias, R. A. *et al.* Sirtuin 4 is a lipoamidase regulating pyruvate dehydrogenase complex activity. *Cell* **159**, 1615–1625 (2014).
9. Madsen, A. S. & Olsen, C. A. Profiling of substrates for zinc-dependent lysine deacylase enzymes: HDAC3 exhibits decrotonylase activity in vitro. *Angew. Chem. Int. Ed.* **51**, 9083–9087 (2012).
10. Aramsangtienchai, P. *et al.* HDAC8 catalyzes the hydrolysis of long chain fatty acyl lysine. *ACS Chem. Biol.* **11**, 2685–2692 (2016).
11. Wei, W. *et al.* Class I histone deacetylases are major histone decrotonylases: Evidence for critical and broad function of histone crotonylation in transcription. *Cell Res.* **27**, 898–915 (2017).
12. Kutil, Z. *et al.* Histone deacetylase 11 is a fatty-acid deacylase. *ACS Chem. Biol.* **13**, 685–693 (2018).
13. Moreno-Yruela, C., Galleano, I., Madsen, A. S. & Olsen, C. A. Histone deacetylase 11 is an ε-*N*-myristoyllysine hydrolase. *Cell Chem. Biol.* **25**, 849–856 (2018).
14. Cao, J. *et al.* HDAC11 regulates type I interferon signaling through defatty-acylation of SHMT2. *Proc. Natl. Acad. Sci. U. S. A.* **116**, 5487–5492 (2019).
15. Olsen, C. A. An update on lysine deacylases targeting the expanding 'acylome'. *ChemMedChem* **9**, 434–437 (2014).
16. North, B. J., Marshall, B. L., Borra, M. T., Denu, J. M. & Verdin, E. The human Sir2 ortholog, SIRT2, is an NAD^+-dependent tubulin deacetylase. *Mol. Cell* **11**, 437–444 (2003).

17. Nagai, T., Ikeda, M., Chiba, S., Kanno, S. I. & Mizuno, K. Furry promotes acetylation of microtubules in the mitotic spindle by inhibition of SIRT2 tubulin deacetylase. *J. Cell Sci.* **126**, 4369–4380 (2013).
18. Dryden, S. C., Nahhas, F. A., Nowak, J. E., Goustin, A.-S. & Tainsky, M. A. Role for human SIRT2 NAD-dependent deacetylase activity in control of mitotic exit in the cell cycle. *Mol. Cell. Biol.* **23**, 3173–3185 (2003).
19. Li, W. *et al.* Sirtuin 2, a mammalian homolog of yeast silent information regulator-2 longevity regulator, is an oligodendroglial protein that decelerates cell differentiation through deacetylating α-tubulin. *J. Neurosci.* **27**, 2606–2616 (2007).
20. Madsen, A. S. *et al.* Investigating the sensitivity of NAD^+-dependent sirtuin deacylation activities to NADH. *J. Biol. Chem.* **291**, 7128–7141 (2016).
21. Galleano, I., Schiedel, M., Jung, M., Madsen, A. S. & Olsen, C. A. A continuous, fluorogenic sirtuin 2 deacylase assay: Substrate screening and inhibitor evaluation. *J. Med. Chem.* **59**, 1021–1031 (2016).
22. Huang, H. *et al.* Lysine benzoylation is a histone mark regulated by SIRT2. *Nat. Commun.* **9**, 3374 (2018).
23. Chalkiadaki, A. & Guarente, L. The multifaceted functions of sirtuins in cancer. *Nat. Rev. Cancer* **15**, 608–624 (2015).
24. Jing, H. *et al.* A SIRT2-selective inhibitor promotes c-Myc oncoprotein degradation and exhibits broad anticancer activity. *Cancer Cell* **29**, 297–310 (2016).
25. Donmez, G. & Outeiro, T. F. SIRT1 and SIRT2: Emerging targets in neurodegeneration. *EMBO Mol. Med.* **5**, 344–352 (2013).
26. Donmez, G. Sirtuins as possible targets in neurodegenerative diseases. *Curr. Drug Targets* **14**, 644–647 (2013).
27. Smith, B. C. & Denu, J. M. Sir2 protein deacetylases: Evidence for chemical intermediates and functions of a conserved histidine. *Biochemistry* **45**, 272–282 (2006).
28. de Oliveira, R. M., Sarkander, J., Kazantsev, A. G. & Outeiro, T. F. SIRT2 as a therapeutic target for age-related disorders. *Front. Pharmacol.* **3**, 82 (2012).
29. Gomes, P., Fleming Outeiro, T. & Cavadas, C. Emerging role of sirtuin 2 in the regulation of mammalian metabolism. *Trends Pharmacol. Sci.* **36**, 756–768 (2015).
30. Outeiro, T. F. *et al.* Sirtuin 2 inhibitors rescue α-synuclein-mediated toxicity in models of Parkinson's disease. *Science* **317**, 516–519 (2007).
31. Eren, G. *et al.* Pharmacophore modeling and virtual screening studies to identify novel selective SIRT2 inhibitors. *J. Mol. Graph. Model.* **89**, 60–73 (2019).
32. Spiegelman, N. A. *et al.* A small-molecule SIRT2 inhibitor that promotes K-Ras4a lysine fatty-acylation. *ChemMedChem* **14**, 744–748 (2019).
33. Ali, T. F. S. *et al.* New SIRT2 inhibitors: Histidine-based bleomycin spin-off. *Bioorg. Med.*

Chem. **27**, 1767–1775 (2019).

34. Yamagata, K. *et al.* Structural basis for potent inhibition of SIRT2 deacetylase by a macrocyclic peptide inducing dynamic structural change. *Structure* **22**, 345–352 (2014).
35. Rumpf, T. *et al.* Selective SIRT2 inhibition by ligand-induced rearrangement of the active site. *Nat. Commun.* **6**, 6263 (2015).
36. Schiedel, M. *et al.* Aminothiazoles as potent and selective SIRT2 inhibitors: A structure-activity relationship study. *J. Med. Chem.* **59**, 1599–1612 (2016).
37. Mellini, P. *et al.* Potent mechanism-based sirtuin-2-selective inhibition by an in situ-generated occupant of the substrate-binding site, 'selectivity pocket' and NAD^+-binding site. *Chem. Sci.* **8**, 6400–6408 (2017).
38. Kudo, N., Ito, A., Arata, M., Nakata, A. & Yoshida, M. Identification of a novel small molecule that inhibits deacetylase but not defatty-acylase reaction catalysed by SIRT2. *Philos. Trans. R. Soc.* B**373**, 20170070 (2018).
39. Yang, L.-L. *et al.* X-ray crystal structure guided discovery of new selective, substrate-mimicking sirtuin 2 inhibitors that exhibit activities against non-small cell lung cancer cells. *Eur. J. Med. Chem.* **155**, 806–823 (2018).
40. Hong, J. Y., Price, I. R., Bai, J. J. & Lin, H. A glycoconjugated SIRT2 inhibitor with aqueous solubility allows structure-based design of SIRT2 inhibitors. *ACS Chem. Biol.* **14**, 1802–1810 (2019).
41. Lain, S. *et al.* Discovery, in vivo activity, and mechanism of action of a small-molecule p53 activator. *Cancer Cell* **13**, 454–463 (2008).
42. Morimoto, J., Hayashi, Y. & Suga, H. Discovery of macrocyclic peptides armed with a mechanism-based warhead: Isoform-selective inhibition of human deacetylase SIRT2. *Angew. Chem. Int. Ed.* **51**, 3423–3427 (2012).
43. Suzuki, T. *et al.* Design, synthesis, and biological activity of a novel series of human sirtuin-2-selective inhibitors. *J. Med. Chem.* **55**, 5760–5773 (2012).
44. Schuster, S. *et al.* A continuous sirtuin activity assay without any coupling to enzymatic or chemical reactions. *Sci. Rep.* **6**, 22643 (2016).
45. Huang, Y., Liu, J., Yan, L. & Zheng, W. Simple *N*ε-thioacetyl-lysine-containing cyclic peptides exhibiting highly potent sirtuin inhibition. *Bioorg. Med. Chem. Lett.* **26**, 1612–1617 (2016).
46. Moniot, S. *et al.* Development of 1,2,4-oxadiazoles as potent and selective inhibitors of the human deacetylase sirtuin 2: Structure-activity relationship, X-ray crystal structure, and anticancer activity. *J. Med. Chem.* **60**, 2344–2360 (2017).
47. Sundriyal, S. *et al.* Thienopyrimidinone based sirtuin-2 (SIRT2)-selective inhibitors bind in the ligand induced selectivity pocket. *J. Med. Chem.* **60**, 1928–1945 (2017).
48. Mellini, P. *et al.* Identification of diketopiperazine-containing 2-anilinobenzamides as potent sirtuin 2 (SIRT2)-selective inhibitors targeting the "selectivity pocket", substrate-binding site,

and NAD^+-binding site. *J. Med. Chem.* **62**, 5844–5862 (2019).

49. Finnin, M. S., Donigian, J. R. & Pavletich, N. P. Structure of the histone deacetylase SIRT2. *Nat. Struct. Biol.* **8**, 621–625 (2001).
50. Moniot, S., Schutkowski, M. & Steegborn, C. Crystal structure analysis of human SIRT2 and its ADP-ribose complex. *J. Struct. Biol.* **182**, 136–143 (2013).
51. Feldman, J. L. *et al.* Kinetic and structural basis for acyl-group selectivity and NAD^+ dependence in sirtuin-catalyzed deacylation. *Biochemistry* **54**, 3037–3050 (2015).
52. Rumpf, T., Gerhardt, S., Einsle, O. & Jung, M. Seeding for sirtuins: Microseed matrix seeding to obtain crystals of human SIRT3 and SIRT2 suitable for soaking. *Acta Cryst.* F**71**, 1498–1510 (2015).
53. Jin, J., He, B., Zhang, X., Lin, H. & Wang, Y. SIRT2 reverses 4-oxononanoyl lysine modification on histones. *J. Am. Chem. Soc.* **138**, 12304–12307 (2016).
54. Knyphausen, P. *et al.* Insights into lysine deacetylation of natively folded substrate proteins by sirtuins. *J. Biol. Chem.* **291**, 14677–14694 (2016).
55. Wang, Y. *et al.* Deacylation mechanism by SIRT2 revealed in the 1′-SH-2′-O-myristoyl intermediate structure. *Cell Chem. Biol.* **24**, 339–345 (2017).
56. Yang, L. L. *et al.* Crystallographic and SAR analyses reveal the high requirements needed to selectively and potently inhibit SIRT2 deacetylase and decanoylase. *Medchemcomm* **10**, 164–168 (2019).
57. Rajabi, N. *et al.* Mechanism-based inhibitors of the human sirtuin 5 deacylase: Structure-activity relationship, biostructural, and kinetic insight. *Angew. Chem. Int. Ed.* **56**, 14836–14841 (2017).
58. Smith, B. C. & Denu, J. M. Mechanism-based inhibition of Sir2 deacetylases by thioacetyl-lysine peptide. *Biochemistry* **46**, 14478–14486 (2007).
59. Smith, B. C. & Denu, J. M. Acetyl-lysine analog peptides as mechanistic probes of protein deacetylases. *J. Biol. Chem.* **282**, 37256–37265 (2007).
60. Dancy, B. C. R. *et al.* Azalysine analogues as probes for protein lysine deacetylation and demethylation. *J. Am. Chem. Soc.* **134**, 5138–5148 (2012).
61. Hirsch, B. M. *et al.* Potent sirtuin inhibition bestowed by L-2-amino-7-carboxamidoheptanoic acid (L-ACAH), a N^{ε}-acetyl-lysine analog. *Medchemcomm* **2**, 291–299 (2011).
62. Rink, H. Solid-phase synthesis of protected peptide fragments using a trialkoxy-diphenyl-methylester resin. *Tetrahedron Lett.* **28**, 3787–3790 (1987).
63. Sadowski, M. *et al.* A synthetic peptide blocking the apolipoprotein E/β-amyloid binding mitigates β -amyloid toxicity and fibril formation in vitro and reduces β-amyloid plaques in transgenic mice. *Am. J. Pathol.* **165**, 937–948 (2004).
64. Rajabi, N., Nielsen, A. L. & Olsen, C. A. Dethioacylation by sirtuins 1–3: Considerations for drug design using mechanism-based sirtuin inhibition. *ACS Med. Chem. Lett.* (2020).

doi:10.1021/acsmedchemlett.9b00580

65. Kawaguchi, M., Ieda, N. & Nakagawa, H. Development of peptide-based sirtuin defatty-acylase inhibitors identified by the fluorescence probe, SFP3, that can efficiently measure defatty-acylase activity of sirtuin. *J. Med. Chem.* **62**, 5434–5452 (2019).
66. Spiegelman, N. A. *et al.* Direct comparison of SIRT2 inhibitors: Potency, specificity, activity-dependent inhibition, and on-target anticancer activities. *ChemMedChem* **13**, 1890–1894 (2018).
67. Moreno-Yruela, C., Madsen, A. S. & Olsen, C. A. Kinetic characterization of inhibitors of histone deacetylases (HDACs) and sirtuins. *Protoc. Exch.* (2019). doi:10.21203/RS.2.13042/V1
68. Schrödinger Release 2019-4: QikProp, Schrödinger, LLC, New York, NY, 2019.
69. Hubbard, B. P. *et al.* Evidence for a common mechanism of SIRT1 regulation by allosteric activators. *Science* **339**, 1216–1219 (2013).
70. Tran, K. T. *et al.* A comparative assessment study of known small-molecule Keap1-Nrf2 protein-protein interaction inhibitors: Chemical synthesis, binding properties, and cellular activity. *J. Med. Chem.* **62**, 8028–8052 (2019).
71. Kitir, B. *et al.* Chemical editing of macrocyclic natural products and kinetic profiling reveal slow, tight-binding histone deacetylase inhibitors with picomolar affinities. *Biochemistry* **56**, 5134–5146 (2017).
72. Jiang, Y., Liu, J., Chen, D., Yan, L. & Zheng, W. Sirtuin inhibition: Strategies, inhibitors, and therapeutic potential. *Trends Pharmacol. Sci.* **38**, 459–472 (2017).
73. Madsen, A. S. & Olsen, C. A. Substrates for efficient fluorometric screening employing the NAD-dependent sirtuin 5 lysine deacylase (KDAC) enzyme. *J. Med. Chem.* **55**, 5582–5590 (2012).
74. Deziel, R., Rahil, J., Wahhab, A., Allan, M. & Nguyen, N. (Methylgene Inc.), *Sirtuin inhibitors*. WO 2009/026701 A1, Mar 5, 2009.
75. Zheng, W. & Jiang, Y. (Jiangsu Univesity), *Selenourea warhead and building method thereof*. CN 106632596 A, May 10, 2017.
76. Lin, H. & Cerione, R. (Cornell University), *Methods for treatment of cancer by targeting SIRT5*. US 2014213530 A1, Jul 31, 2014.
77. Suga, H. & Morimoto, J. (The University of Tokyo). *Peptide library production method. peptide library, and screening method*. US 10195578 B2, Feb. 5, 2019.
78. Lin, H. (Cornell University). *Thiourea compounds and their use as inhibitors of SIRT2 or SIRT5*. US 10556878 B2, Feb 11, 2020.
79. Dai, H., Sinclair, D. A., Ellis, J. L. & Steegborn, C. Sirtuin activators and inhibitors: Promises, achievements, and challenges. *Pharmacol Ther.* **188**, 140–154 (2018).
80. Li, S., Wu, B. & Zheng, W. Cyclic tripeptide-based potent human SIRT7 inhibitors. *Bioorg. Med. Chem. Lett.* **29**, 461–465 (2019).

81. Dodge, A. G., Richman, J. E., Johnson, G. & Wackett, L. P. Metabolism of thioamides by *Ralstonia pickettii* TA. *Appl. Environ. Microbiol.* **72**, 7468–7476 (2006).
82. Poulsen, L. L., Hyslop, R. M. & Ziegler, D. M. *S*-oxygenation of *N*-substituted thioureas catalyzed by the pig liver microsomal FAD-containing monooxygenase. *Arch. Biochem. Biophys.* **198**, 78–88 (1979).
83. Zaorska, E. *et al.* Evaluation of thioamides, thiolactams and thioureas as hydrogen sulfide (H_2S) donors for lowering blood pressure. *Bioorg. Chem.* **88**, 102941 (2019).
84. Skoge, R. H. & Ziegler, M. SIRT2 inactivation reveals a subset of hyperacetylated perinuclear microtubules inaccessible to HDAC6. *J. Cell Sci.* **129**, 2972–2982 (2016).
85. Hu, F. *et al.* Inhibition of SIRT2 limits tumour angiogenesis via inactivation of the STAT3/VEGFA signalling pathway. *Cell Death Dis.* **10**, 9 (2019).
86. Li, Y. *et al.* SIRT2 promotes the migration and invasion of gastric cancer through RAS/ERK/JNK/MMP-9 pathway by increasing PEPCK1-related metabolism. *Neoplasia* **20**, 745–756 (2018).
87. Chen, J. *et al.* SIRT2 overexpression in hepatocellular carcinoma mediates epithelial to mesenchymal transition by protein kinase B/glycogen synthase kinase-3β/β-catenin signaling. *Hepatology* **57**, 2287–2298 (2013).
88. Spiegelman, N. A. *et al.* SIRT2 and lysine fatty acylation regulate the activity of RalB and cell migration. *ACS Chem. Biol.* **14**, 2014–2023 (2019).
89. Tharp, J. M. *et al.* An amber obligate active site-directed ligand evolution technique for phage display. *Nat. Commun.* **11**, 1392 (2020).
90. Galleano, I., Nielsen, J., Madsen, A. S. & Olsen, C. A. Scalable and purification-free synthesis of a myristoylated fluorogenic sirtuin substrate. *Synlett* **28**, 2169–2173 (2017).
91. Kabsch, W. *et al.* XDS. *Acta Cryst.* D**66**, 125–132 (2010).
92. Vagin, A. & Teplyakov, A. MOLREP: An automated program for molecular replacement. *J. Appl. Crystallogr.* **30**, 1022–1025 (1997).
93. Winn, M. D. *et al.* Overview of the CCP4 suite and current developments. *Acta Cryst.* D**67**, 235–242 (2011).
94. Murshudov, G. N. *et al.* REFMAC5 for the refinement of macromolecular crystal structures. *Acta Cryst.* D**67**, 355–367 (2011).
95. Emsley, P., Lohkamp, B., Scott, W. G. & Cowtan, K. Features and development of Coot. *Acta Cryst.* D**66**, 486–501 (2010).
96. Long, F. *et al.* AceDRG: A stereochemical description generator for ligands. *Acta Cryst.* D**73**, 112–122 (2017).
97. Chen, V. B. *et al.* MolProbity: All-atom structure validation for macromolecular crystallography. *Acta Cryst.* D**66**, 12–21 (2010).

Acknowledgements

We thank Michael Bæk, Dr. Iacopo Galleano, and Dr. Martin Roatsch for donation of building blocks, as well as Julie E. Bolding and Kathrin S. Troelsen for assistance with cell culture experiments. We thank Professor Thue W. Schwartz for access to equipment for performing invasion/migration experiments. The pCDH-SIRT2-Flag vector was a gift from Professor Hening Lin (Addgene plasmid #102624) and the pCDNA3.1-eGFP-Flag vector was a gift from Professor Stephan A. Pless. The X-ray crystallography was performed under the approval of the Photon Factory Program Advisory Committee (Proposal No. 2017G662, and 2019G669, and PSI Proposal No. 20181219, 20181299). This work was supported by JSPS KAKENHI (JP19H05640; M.Y.), the Lundbeck Foundation (Running cost grant R289-2018-2074; CAO), the Carlsberg Foundation (2013-01-0333, CF15-011, and CF18-0442; C.A.O.), the Novo Nordisk Foundation (NF17OC0029464; C.A.O.), and the European Research Council (ERC-CoG-725172–*SIRFUNCT*; C.A.O.). We thank the COST-Action CM1406 (EPICHEMBIO) for support.

Author contributions

A.L.N, N.R., and C.A.O conceptualized the study; A.L.N., N.R., M.F., and A.L. performed the chemical synthesis and biochemical characterization; A.L.N. and K.L. performed the cell-based assays; A.L.N. performed the formal analysis of the raw data; N.K. obtained the crystals and solved the structures; A.L.N. and C.A.O wrote the original draft of the manuscript; all authors reviewed and edited the final manuscript; C.A.O. acquired funding. A.S.M., M.Y., and C.A.O. supervised the study.

Additional information

Accession codes: X-ray diffraction data, coordinates, and structure factors for the X-ray crystal structures are deposited with the PDB (www.wwpdb.org) under the accession numbers 7BOS (SIRT2:**13**) and 7BOT (SIRT2:**23**).

Supplementary Information accompanies this paper

Competing interests

The authors declare no competing financial interest.

ORCID:

Alexander L. Nielsen: 0000-0003-1195-0143

Nima Rajabi: 0000-0002-9509-7540

Norio Kudo: 0000-0001-6468-7006

Kathrine Lundø: 0000-0002-6566-9317

Andreas S. Madsen: 0000-0001-7283-2090

Minoru Yoshida: 0000-0002-4376-5674

Christian A. Olsen: 0000-0002-2953-8942